EUROPEAN ORGANIZATION FOR NUCLEAR RESEARCH

CERN-TH 6452
IFAE-92/001

Neutrino Fluxes at Future Hadron Colliders

A. De Rújula[1], E. Fernández[2] and J.J. Gómez-Cadenas[1]

[1] *CERN-CH-1211 Geneva 23, Switzerland*
[2] *Institut de Física d'Altes Energies*
08193 Bellaterra, Barcelona, Spain

Abstract

We study the neutrino fluxes produced by the decay of low momentum transfer charmed and beautiful particles in beam-beam and fixed-target collisions at LHC and SSC energies. To study the total production cross-sections and longitudinal momentum distribution of those particles, we use a non-perturbative QCD approach, the Quark Gluon String Model. The transverse momentum distributions are computed by extrapolation of existing data with an empirical formula based on Hagedorn's thermodynamical model. We discuss various set-ups to detect and exploit these neutrinos at the LHC. We find that in a relatively small target located directly downstream of the interaction point, at about 100 metres distance, a few thousand ν_τ interactions per year, at the current design luminosity of the LHC, could be observed. The number of ν_e and ν_μ interactions will be a factor of 10 higher. This demonstrates the possibility of a high energy neutrino physics program at the LHC (and possibly also at the SSC) that would include a direct observation of the yet unseen tau neutrino.

CERN-TH 6452
IFAE-92/001
April 1992

1 Introduction

Elementary scalars and the top quark are customarily mentioned as the two building blocks of the Standard Model to be searched for at the LHC and the SSC. Remarkably, the same colliders could also make possible a rich neutrino physics program including the direct observation of the tau neutrino, presumably for the first time.

Unlike ν_e and ν_μ neutrino beams, which come from the decays of particles copiously produced at present facilities, intense ν_τ beams are more difficult to generate. Present experiments trying to observe tau neutrinos [1, 2, 3] have to rely, alas, on the possibility of ν_μ-ν_τ oscillations. But, as pointed out in ref. [4], intense, collimated beams of fast-decaying charmed and beautiful particles are a free bonus of future hadron colliders. These particles, particularly D_s mesons, will be a source of tau neutrinos. To estimate how intense and collimated the resulting ν_τ beams are, it is necessary to have a model that describes low transverse momentum ($p_\perp$) charm and beauty production at very high energies.

The beam-beam interactions at future hadron colliders *unavoidably* generate intense and naturally collimated neutrino and antineutrino beams of the various flavours. Prompt-decay beams of comparable properties can also be produced in fixed-target collisions at these facilities, for instance in beam-scrapers or in a dedicated beam dump. Thus, we shall compute ν_e, ν_μ and ν_τ fluxes at four center-of-mass energies, namely $\sqrt{s} = 123.2$ GeV (LHC, 8 TeV protons on a fixed target), $\sqrt{s} = 197.7$ GeV (SSC, 20 TeV protons on a fixed target), $\sqrt{s} = 16.0$ TeV (LHC beam-beam, 8×8 TeV protons), and $\sqrt{s} = 40.0$ TeV (SSC beam-beam, 20×20 TeV protons). We shall neglect throughout the relatively small [4] contribution to neutrino fluxes from the decays of pions, kaons and hyperons. Most of these particles hit one collider component or another well before their characteristic decay time.

Perturbative QCD provides a fairly good description of the experimental data (see the reviews in [5]) on the photoproduction and electroproduction of charmed particles. Understandably, the use of analogous perturbative methods to calculate in detail the production of charmed particles in hadron-hadron collisions fails to describe the data, although calculations to increasing orders in α_s appear to improve the situation [6]. The perturbatively calculated total production cross-section and longitudinal-momentum distribution of charmed particles differ significantly from those obtained experimentally, as they should: charmed particles as well as lighter hadrons are produced mainly at small transverse momentum ($p_\perp \sim 1$ GeV), a region wherein perturbative QCD is expected to fail.

In this paper we calculate the production cross-sections for charmed and beautiful particles using a non-perturbative QCD approach to the description of hadron processes, the Quark Gluon String Model, QGSM (see [10] below and references therein). This approach has been applied with amazing success to the production of hadrons containing light u, d and s quarks, and it has been shown to describe adequately the production of charmed mesons at the explored low and moderate energies.

The QGSM, which we briefly review for the sake of self-containment in Section 2, is not a "theory" swiftly following from first principles. Rather, it is a pot-pourri of quark-

parton model ideas, QCD string dynamics and Reggeon calculus. Its redeeming value, as that of any other recipe, is to be judged from its practical success and the good taste and simplicity of its input ingredients. Also in Section 2, cross-sections and longitudinal momentum distributions for charmed meson production are computed, compared with existing data and extrapolated to the high energies that are relevant here. We also calculate the QGSM cross-sections for the production of beautiful mesons. The uncertainty of the model predictions is more serious in this case, but the contribution of beauty production to the neutrino interaction rates of interest to us is only at the level of 5 to 15%.

To compute neutrino fluxes at unexplored energies, a prediction for the evolution with energy of the $p_\perp$ distributions of charmed and beautiful particles is needed. The QGSM has not yet been extended to a description of $p_\perp$ distributions, and we rely on an empirical parametrization of ours, based on Hagedorn's thermodynamical model [7] and meant to *pessimize* the expectations for neutrino counting rates. The parameters are obtained by fitting the available data on average $p_\perp$ distributions for the production of hadrons of different masses, in the manner we discuss in Section 3. The expected neutrino fluxes at the LHC and SSC, both in fixed-target and beam-beam collisions, are computed in Section 4. In order to give a flavour for the feasibility of such an experiment, we briefly discuss in Section 5 the issue of ν_τ detection and compute the expected number of neutrino interactions in a rather small detector designed to fit in the long straight section of the LHC, a mere 100 m from the interaction point. We present our conclusions in Section 6.

2 The Quark Gluon String Model

The QGSM is a non-perturbative parton-model approach to the description of hadron processes. It is based on the topological $1/N_f^2$ expansion (with N_f the number of quark flavours) of quantum chromodynamics [8, 9] and the string model of hadronic reactions. In the QGSM, the graphs of the $1/N_f^2$ expansion correspond to a definite space-time picture of quark interactions and of the production and fate of quark-gluon strings. Among other important applications [10], the model can be used to describe in great detail and in terms of very few parameters the multiple production of hadrons in hadron-hadron and hadron-nucleus collisions, including particle multiplicity and multiplicity distributions for different flavours, longitudinal momentum distributions, the KNO scaling and deviations thereof, the t dependence of elastic cross-sections and the ratio of the corresponding real and imaginary amplitudes in the forward direction.

The basic picture of the QGSM is that the bulk of the production of hadrons at moderate and high energies is described by "cutting" the forward scattering diagrams of the "cylindrical" type shown in Fig. 1a. Each cylinder corresponds to the exchange of a single Pomeron. This picture is a modification of the planar case of Fig. 1b, involving the annihilation of some of the valence quarks of the colliding hadrons and corresponding to subdominant Regge trajectories. In the planar case a single configuration of the colour-string type appears in the final state of the inelastic scattering amplitude, as illustrated in Fig. 1c. In the cylindrical case, one or various gluons are exchanged, as opposed to a valence quark, leading to the formation of two strings as in Figs. 1d, which illustrates the two cuts required to slice vertically the cylindrical diagram of Fig. 1a. Each of the two chains of hadrons in the final state should be similar to the single chain of the

planar case in Fig. 1b. The QGSM also deals with the exchange of several Pomerons in the t channel, a process whose relevance increases with energy. Multi-pomeron diagrams correspond to the succesive terms of the $1/N_f^2$ expansion. Figure 1e succinctly illustrates how multipomeron or multichain processes result from the non-valence constituency of the colliding hadrons.

To calculate the cross-sections for the production of secondary particles, it is necessary to know the distribution functions of the "dressed" quarks (the ends of the strings) in the colliding hadrons, as well as the fragmentation functions of these quarks into secondary hadrons. In dealing, as we shall, with pp collisions, the diquark structure and fragmentation functions are also needed. In the QGSM, it is assumed that all these functions are determined in the (Feynman variable) $x \to 0$ and $x \to 1$ limits [11] by the corresponding Regge asymptotic behaviour, and at intermediate x by the simplest interpolation: the product of the two asymptotic behaviours. In contradistinction to other "particle generators" the model satisfies all the relevant conservation laws. For example, the sum of the momenta of all the constituents of a hadron is equal to the momentum of the hadron. The momentum is also conserved in processes of fragmentation of quarks and diquarks into secondary hadrons. In addition, in the case of fragmentation of quark-diquark and quark-antiquark strings, the electric and baryon charges, as well as strangeness and the other flavour quantum numbers, are conserved.

In the QGSM the inclusive cross-section for the production of a hadron h (see [12] and references therein) is:

$$\begin{aligned} f = \frac{d\sigma^h}{dy} &= \hat{x}\frac{d\sigma^h}{dx} = \\ \int E\frac{d^3\sigma^h}{d^3p}d^2p_\perp &= \sum_n \sigma_n(s)\phi_n^h(s,y), \end{aligned} \tag{1}$$

with the conventional definitions

$$\begin{aligned} y &\equiv \frac{1}{2}\ln\frac{(E+p_\parallel)}{(E-p_\parallel)}, \\ x &\equiv \frac{2p_\parallel}{\sqrt{s}}, \\ \hat{x} &\equiv \frac{2E}{\sqrt{s}} = \sqrt{x^2 + 4m_h^2/s} \end{aligned} \tag{2}$$

and with $\sigma_n(s)$ the cross-section for producing the $2n$ chains appearing in the cutting of n-cylinder diagrams. The expressions for $\sigma_n(s)$ have been obtained in [11, 10]. In Fig. 2 we show the dependence of the total pp cross section with energy. Differential cross-sections involve the functions $\phi_n^h(s,y)$, the distributions over rapidity y of the hadron h in the $2n$-chain process. These functions can be written as a convolution of the quark and diquark distribution functions in the colliding hadrons, $f^{q(qq)}$, with the fragmentation distributions $D^h_{q(qq)}(x/x_1)$ of the quarks and diquarks into the hadron h. In the case of interest to us (pp interaction to produce charmed hadrons), we can write

$$\begin{aligned} \phi_n^D(s,x) &= a_0^D(F_q(x_+)F_{qq}(x_-) + F_q(x_-)F_{qq}(x_+) + \\ &\quad 2(n-1)F_{q_{sea}}(x_+)F_{q_{sea}}(x_-)), \end{aligned} \tag{3}$$

where

$$\begin{aligned} x_\pm &\equiv 1/2\sqrt{x_\perp^2 + x^2} \pm x \\ x_\perp &\equiv 2m_h/\sqrt{s}. \end{aligned} \tag{4}$$

The functions $F_i(x_\pm)$ are then

$$F_i(x_\pm) = \int_{x_\pm}^1 dx_1 f^i(x_1,n) D_i\left(\frac{x_\pm}{x_1}\right), \tag{5}$$

where $f^i(x_1,n)$ is the structure function of quark i, having a fraction of the energy x_1 of the interacting hadrons, and $D_i(z)$ is the fragmentation function of the quark chain into a hadron of fractional energy z. The structure functions f^i would (from the point of view of their deep-inelastic-scattering counterparts) correspond to the "naïve" parton-model scale of momentum transfers of the order of an inverse hadronic radius. The distribution functions $f^i(x_1)$ of the quarks (diquarks) can be written in terms of the intercepts $\alpha_R \sim 0.5, \alpha_N \sim -0.5$, of known Regge poles. For example,

$$f_p^u(x_1,n) = C_u(n)x_1^{-\alpha_R}(1-x_1)^{\alpha_R - 2\alpha_N + n - 1}. \tag{6}$$

A complete list of the functions $f^i(x_1)$ and the values of their various parameters are given in ref. [12].

The QGSM fragmentation function into charmed mesons is determined as $z \to 1$ by α_ψ – the intercept of the $c\bar{c}$ Regge trajectory – on which we have no direct empirical information. If one assumes that, as in the case of light quarks, the $c\bar{c}$ trajectories are linear and exchange-degenerate, then, from the masses of the $2^+\chi(3555)$ and $1^-\psi(3100)$ states, the slope of the ψ trajectory is $\alpha'_\psi \sim 0.33$ GeV^{-2} and its intercept $\alpha_\psi \sim -2.2$. On the other hand, it may be supposed that the parameters of the ψ trajectory are dictated by perturbation theory on QCD. In this case $\alpha_\psi \sim 0$ and the trajectory should be strongly non-linear [13]. We shall consider the linear and perturbative values as defining the extremes of our spectrum of possibilities.

Consider the fragmentation of various quark (diquark) chains into D-mesons, for which there are various quark configurations, as illustrated in Fig. 3. For the fragmentation of the u-quark chain into $\bar{D}^0$ mesons (favoured fragmentation, see Fig. 3), for instance we have:

$$D_u^{\bar{D}^0} = a_o^D(1-z)^{-\alpha_\psi + \lambda}(1 + a_1 z^2), \tag{7}$$

while for the (unfavoured) fragmentation of the u-quark chain into a D^+ meson:

$$D_u^{D^+} = a_o^D(1-z)^{-\alpha_\psi + \lambda + 2(1-\alpha_R)}, \tag{8}$$

Here z is the fraction of energy carried by the charmed meson and $\lambda \sim 0.5$ [13]. The full list of fragmentation functions and all of the parameter values are given in ref. [13].

The QGSM has been quite successful in explaining the existing data [10, 14] on cross-sections, x and y spectra, multiplicity distributions and other features of the data such as the deviations from KNO scaling. It also describes quite well the scarce experimental data

on charm production [13, 15]. The cleanest and most reliable data on charmed meson production have been obtained by the LEBC-EHS and the LEBC-MPC collaborations. The LEBC-EHS group has measured the inclusive charmed meson production in πp [16] collisions at $\sqrt{s} = 24.3$ GeV and the inclusive and exclusive $(D^+, D^-, D^0, \bar{D}^0)$ charmed-meson production in pp collisions [17, 18] at $\sqrt{s} = 27.4$ GeV, while the LEBC-MPS collaboration observed the inclusive production of D mesons in pp collisions [19] at $\sqrt{s} = 38.8$ GeV. The only data on charm production at high energy [20], $\sqrt{s} = 630$ GeV, has been obtained by measuring the production of prompt electrons of relatively low $p_\perp$ (0.5-2 GeV) in the CERN $p\bar{p}$ collider.

In Fig. 4 we show the differential cross-sections (expressed in the invariant form $\hat{x}d\sigma/dx$) for the different D mesons measured by LEBC-EHS, [18] and compare them with the QGSM predictions for $\alpha_\psi = 0$ and $\alpha_\psi = 2.2$. The cross-sections for the charged $D^\pm$ mesons are well described by the theory, while the data on $D^0(\bar{D}^0)$ distributions are significantly harder (softer) than the model predictions. As pointed out in ref. [18] this can be the result of bad particle identification: the existence of 16 $D^0/\bar{D}^0$ ambiguous decays with a hard x distribution compared with the 29 D^0 and 22 $\bar{D}^0$ candidates introduced an important source of uncertainty on the measurement. Notice that in pp interactions at (relatively) low energy we would expect $\bar{D}^0(u\bar{c})$ to have a harder spectrum than $D^0(\bar{u}c)$, since the former meson can be produced directly on the leading u quarks of the colliding protons. In the QGSM the fragmentation function for D^0 production (see Fig. 3.c) is suppressed by a factor $\sim (1-x)^{2\alpha_R - 2\alpha_N}$ relative to that $\bar{D}^0$. Figure 4 shows that the predictions of the QGSM for the two possible values of α_ψ are very similar.

In Fig. 5 we show the inclusive spectra of D mesons measured by LEBC-MPS [19] together with the model predictions. Again, the data are fairly well described with both values of α_ψ. In Fig. 6 the QGSM prediction for the evolution of the total cross-section $\sigma(D\bar{D})$ with energy is shown and compared with the measurements of the cited LEBC experiments. At high energies, the predictions for $\alpha_\psi = 0$ and 2.2 differ by a factor close to 3. Unfortunately, the large error in the charm cross-section measurement at $\sqrt{s} = 630$ GeV does not allow one to extract a useful constraint on α_ψ. The predictions for the x distributions of D_s mesons at the four centre-of-mass energies of interest at the LHC and SSC are shown in Fig. 7. The figure illustrates how the predicted increase of the cross-section with energy is predominantly a low-x effect. Thus, since the neutrino interaction cross-section is roughly linear with energy, the predictions for the number of neutrino interactions are quite insensitive to the value of α_ψ. In Table 1 we compare the measured total cross-sections for charmed-particle production with the model predictions.

An interesting point concerns the evolution with energy of the cross-sections and x distributions for the different exclusive states $D^\pm, D^0, \bar{D}^0$ and $D_s^\pm$. If the "leading" constituent-quark effect constitutes a dominant feature, one expects a harder spectrum and larger cross-sections for $\bar{D}^0$ and D^- than for D^0 and D^+. The production of $D_s^\pm$, where an additional $s\bar{s}$ chain has to be produced, is expected to be more suppressed still. But the increase of cross-sections with energy occurs essentially at very low x and in the limit of very high energy (LHC or SSC beam-beam modes) the individual charmed-meson cross-sections (including D_s) are predicted to behave in the flavour-democratic fashion illustrated in Fig. 8, wherein we show the model predictions (for $\alpha_\psi = 0$) for the various

x distributions at the four relevant centre-of-mass energies.

The QGSM can also be used (or somewhat abused) to describe the production of beauty. One practical problem is that the intercept α_Υ of the beautiful-meson Regge trajectory has an even larger uncertainty than that of α_ψ. As usual the parameters of a linear trajectory can be reconstructed from the resonances, in this case $\Upsilon(9460), \Upsilon(10023)$ and $\chi(9915)$. Following ref. [15] we take $\alpha_\Upsilon = -8$ or 0 for the case of a linear or non-linear trajectory, respectively. In Fig. 6 the QGSM prediction for the evolution of the total cross-section $\sigma(b\bar{b})$ with energy is shown for these values of α_Υ. In Fig. 9 we show the predicted B^+ x distribution at the four centre-of-mass energies considered. As for charmed mesons the differences are largely erased in the prediction for neutrino interactions; the model with the higher cross-section also has a softer energy distribution.

To summarize, the QGSM is the most satisfactory of the tools available to describe charm production at modest momentum transfers. It describes well an impressive number of features of hadronic interactions and all the recent data on charm production at all the available energies. It can also be applied to describe beauty production, although with much larger uncertainties in the results, the input parameters and, not least, the theoretical justification. The QGSM makes possible a calculation of the neutrino flux produced by the prompt decay of the charmed-particles produced at the LHC and the SSC. That the B-induced flux is not predictable theoretically (with the same confidence) is not a serious problem; we will end up neglecting it, and it can only help.

3 The Transverse Momentum Distribution of Charmed Particles

The QGSM has not been developed to the point of predicting the transverse momentum spectrum of the produced hadrons. And not only do current experimental data pertain to small energies compared with those of the LHC or SSC beam-beam modes, but for charmed particles the data are rather scarce.

To describe the transverse momentum distributions for the production of particles of mass m in the forward-backward cones of interest to neutrino physics, we adopt the classical thermodynamical model of Koppe [21] and Fermi [22], as elaborated by Hagedorn [7] and collaborators. In this model the $p_\perp$ distributions are essentially exponential in m_T/T, with $m_T = \sqrt{p_\perp^2 + m^2}$ the "transverse mass", and T a "temperature" depending exclusively on the centre-of-mass energy:

$$\frac{d\sigma}{dp_\perp} \propto p_\perp T \sqrt{m_T}\ e^{-\frac{m_T}{T}}. \tag{9}$$

With this expression we have fitted the existing data on the average transverse momentum of charged pions, kaons and antiprotons, for various trial functions $T(s)$. A reasonable fit for which $\langle p_\perp \rangle$ increases fast above the explored energies (a *pessimistic* choice, as far as neutrino physics is concerned) is given by:

$$T = a + b\left(log\,\frac{s}{s_0}\right)^c$$

where a, b and c are constants, *independent* of the particle mass and s_0 is 1 $(\mathrm{GeV/c})^2$. The numerical values of these constants are found to be:

$$\begin{aligned} a &= 0.128 \pm 0.002 \text{ GeV} \\ b &= (1.5 \pm 1.4) \times 10^{-8} \mathrm{GeV} \\ c &= 5.9 \pm 0.8, \end{aligned}$$

the parameters b and c being strongly correlated.

The behaviour of $\langle p_\perp(m,s)\rangle$ is illustrated in Fig. 10, wherein the data for π, K and $\bar{p}$ are from ref. [23], the dashed and dotted curves are the predictions of the formula for the average $p_\perp$ of charmed and beautiful particles, respectively, and the existing data point for charmed particles at $\sqrt{s} = 28$ GeV [16, 17, 18] is also shown. At small energies $T(s)$ is practically constant and $\langle p_\perp\rangle$ depends only on m. At intermediate s, $T(s)$ begins to grow significantly and so do the various $\langle p_\perp(m)\rangle$. The mass of the produced particles becomes almost irrelevant at very high energies, as the various $\langle p_\perp\rangle$ merge into a common curve. From our fits to eq. (7) the predictions of $\langle p_\perp\rangle$ for charmed particles at LHC colliding energies is 2 ± 1 GeV/c and 3 ± 2 GeV/c for SSC collisions. For bottom particles these values are 3 ± 1.5 GeV/c at the LHC and 4 ± 2.5 GeV/c at the SSC.

4 Neutrino Fluxes

Once the yield, longitudinal- and transverse-momentum distributions for charmed and beautiful particles are known, the calculations of the neutrino fluxes produced by their decays can be carried out. The beauty production cross-section is not negligible, but the detectors of modest transverse size that we shall consider would miss a large fraction of the beauty-decay neutrinos, given their considerable transverse momentum. Their contribution to the final neutrino counting rate is only at the level of a few percent of the charm-induced rates. Therefore the main source of neutrinos is charmed particles. We have neglected the relatively very soft neutrino flux (dominantly ν_μ) due to the decay of pions, kaons and hyperons; only a very small fraction of these particles decay before they hit the beam pipe, the magnets or the plugs. We have also neglected (for lack of input data) the production and decay of charmed baryons and we therefore concentrate on the inclusive production of $D^+, D^-, D^0, \bar{D}^0, D_s^+$ and D_s^-. While ν_es and ν_μs are produced in the semileptonic decays of all the above mesons, ν_τs are only copiously produced either in the leptonic decay of the D_s ($D_s \to \tau\nu_\tau$), or in the subsequent tau decay. The D_s–decay neutrino ν_τ^1 has a relatively low energy, owing to the small difference between the τ and D_s masses, while the neutrino produced by the decay of the τ (ν_τ^2) has on the average a larger energy.

The flux calculations were done with a Monte Carlo program that generates D and B mesons with cross-sections and x distributions given by the QGSM and $p_\perp$ distributions as described in sections 2 and 3. The produced mesons were allowed to decay according to the Lund Monte Carlo [24]. We have used the experimentally measured branching ratios for $D^+, D^0 \to e^+ + X$ [25], and assumed the same branching ratio for $D^+, D^0 \to \mu^+ + X$ and $D_s^+ \to e^+(\mu^+) + X$. For the branching ratio of the decay $D_s \to \tau\nu_\tau$, we use 4%, the result reported in [26]. The branching ratios for all B decays are computed in terms of

the naïve spectator approach. Table 2 shows the branching ratios we use for the different decay modes.

Figure 11 shows $z_\nu dN_\nu/dz_\nu$ distributions ($z = E_\nu/E_{beam}$) in an arbitrary scale for the four energies of interest and for $\nu_e(\nu_\mu)$ and ν_τ (or their antiparticles). Since the neutrino interaction cross-section is roughly linear in E_ν and the neutrino beams are naturally collimated in the forward direction, the quantity of choice (besides the energy-weighed flux) is $E_\nu(cos\theta)dN_\nu/dcos\theta$, which we display in Fig. 12 for the same four consuetudinary energies. From these distributions the neutrino interaction rates can be obtained in a detector covering a given fraction of the solid angle. Figure 12 indicates that the e-folding aperture of the neutrino beam from fixed-target LHC collisions is of the order of 1.5 mrad. It decreases to ~ 1 mrad as one moves to SSC fixed-target collisions; the average $p_\perp$ has changed little and the extra boost makes the beam narrower. At $\sqrt{s} = 16$ TeV the x distribution is predicted to be much softer and the $p_\perp$ distribution considerably wider than at the lower energies, conspiring to bring the beam aperture back to some 1.5 mrad. Once again, the predicted $p_\perp$ and x distributions change little from $\sqrt{s} = 16$ to 40 TeV and the beam narrows down to a characteristic 1 mrad aperture at the higher energy.

In the next section we discuss some specific examples of detectors radially subtending (at their up stream end) 2 mrad of the neutrino beam(s). To give a feeling for their response, we illustrate in Fig. 13 the scatter plot of energy versus angle of tau neutrinos produced in LHC beam-beam interactions, as well as their energy distribution, integrated over emission angles. The third plot in this figure illustrates the energy distribution of neutrinos having interacted in a detector of the aforementioned radial transverse size (2 mrad). The facts that the energetic neutrinos tend to be the forward ones and that the neutrino cross-sections are roughly linear with energy make the spectrum of interacting neutrinos very significantly harder than the unrestricted one. Also, the predicted rise in charm-production cross-sections occurs mainly at low x, and an increasing fraction of neutrinos is lost to the low-energy large-angle component, as the parental collision energy is incresed. But at all energies, and for a fixed weight, a long and narrow detector is always the optimal one, an admittedly obvious fact.

5 Possible Neutrino Experiments at the LHC

As an application of the above calculations we consider specific examples of experimental set-ups at the LHC and compute the corresponding neutrino-interaction rates. For completeness we also give numbers for the SSC, where similar set-ups could be conceivably envisaged.

The identification of ν_e and ν_μ charged-current events will be based, as in present detectors, on the observation of the charged lepton. The techniques are well known and valid at LHC (SSC) energies.

The detection of ν_τ at high energies may be based on a variety of techniques. A first possibility is to exploit the fact that the produced τ's will in general fly a considerable distance (of the order of 1 cm) before decaying. This decay length has a broad distribution because of the wide ν_τ energy spectrum. Contrariwise, the transverse decay length and the transverse impact parameter (of a track produced in the decay $\tau \to 1$ charged particle $+ X$, with branching ratio 86%) with respect to the primary vertex are nearly

invariant, with a mean value of about 250 μm. We illustrate these concepts in Fig. 14. Figure 14a shows the energy spectrum of the τ's produced by a ν_τ CC interaction in a forward detector intercepting 2 mrad of radial aperture of the ν beam produced in pp collisions at the LHC collider, at a centre-of-mass energy of 16 TeV. Figure 14b shows the distribution of the paths of the produced τ's. Figure 14c shows the distribution of transverse decay lengths.

Detectors aimed at the observation of secondary vertices or at the measurement of transverse impact parameters have to be very fine-grained. Several possibilities have been discussed [27]. Compact, very finely segmented detectors of relatively high density (i.e. 2 g/cm^3) could be based on bundles of scintillating fibres (of some 20 μm diameter) oriented in the direction of the ν beam. They could also consist of alternating layers of live targets (glass hodoscopes) and micro-strip detectors (silicon or scintillating fibres). Alternatively, one can skirt the observation of the track of a τ, focus on events with a charged lepton ($l = e, \mu$) in the final state, and sieve the ν_τ events with simple kinematical criteria [1]. The signal ($\nu_\tau \to \tau \to l\nu\bar{\nu}$) contains a large missing transverse momentum ($P_\perp^{miss}$) while the bulk of the background ($\nu_l \to l$) does not. The main background giving $P_\perp^{miss} \neq 0$ (the $\nu_l$induced CC production of charmed particles) differs from the signal in the angular distributions (in the transverse plane) of $P_\perp^{miss}$, the lepton momentum (P_l), and the sum of the hadron momenta (P_h). The event distributions in the angles $\phi_{m,h}$ (between $P_\perp^{miss}$ and P_h) and $\phi_{l,h}$ (between P_l and P_h as in Fig. 15) are a powerful tool to discriminate between signal and background. Figure 16, from [1], shows the scatter plot ($\phi_{\mu,h}, \phi_{m,h}$) for ν_μ and ν_τ interactions at the LHC (beam-beam mode). The line indicates the region of the ($\phi_{\mu,h}, \phi_{m,h}$) plane, where ν_τ interactions can be detected with high efficiency and very low background. The disadvantege of the currently planed version of such a device is its very low density. Another interesting possibility for τ identification could be the observation of a jump in ionization in the decay $\tau \to$ 3 charged tracks, which could be achieved with use of an "Icarus-like" [28] liquid-argon TPC, a completely active and rather dense detector.

In Fig. 17 we show the proposed scheme of the LHC 450-m-long straight sections [29]. A possible experimental location is an existing or newly excavated cavern adjacent to the main tunnel, downstream of the first bending dipoles, at the beginning of the collider's arches. Figure 12 indicates that in order to intercept a sizeable fraction of the neutrino flux (e.g. 2 mrad in the forward direction) this detector, located some 500 m away from the interaction point, should have a transverse diameter of about 1 m. High energy "conventional" ν_e and ν_μ physics, where secondary vertex detection is not needed, could be merrily pursued in this location, and so could perhaps ν_τ detection with kinematical selection [1] or with a denser bubble-chamber-like device [28]. The finer-grain ν_τ-identification techniques would make such a large detector prohibitively expensive.

To detect the ν_τ by observing the τ flight one way or another, it might be financially wiser to locate the detector much closer to the interaction point. This possibility exists at the LHC. Figure 17 shows that at about 100 m from the interaction point (after the dipole D_2) the two proton beams have come apart to circulate in rings separated by 18 cm. The empty space between the two beam pipes (about 10 cm) subtends here an angle of 1 mrad and is directly forward from the interaction point. This region could be used to locate the fine-grained central part of a detector, perhaps to be completed

with other elements, located around the beam pipes, as schematically shown in Fig. 18. Neutrino physicists may not be accustomed to hugging detectors around beam pipes, but collider experts make a living of it. Even two beam pipes would not scare an ISR old-timer. Given the small size of this detector, one can afford the use of highly segmented components. The dipole magnets deflect charged particles up to energies close that of the LHC beam, thus reducing enormously the background coming from very forward charged secondaries. Also shown in Figs. 17 and 18 are the plugs P, a few tens of metres of dense material supposed to reduce the neutral-particle radiation on the accelerator components downstream of the D_1 dipole. These plugs are also a shield for a possible ν detector located in this neighbourhood. We have not yet attempted to analyse in detail the residual backgrounds, nor the active ways to suppress them.

Here we will simply compute the interaction rates for ν_μ (ν_e) and ν_τ in the active target of a generic detector subtending 2 mrad in the forward direction, 40 m long and with an average density of 2 g/cm^3. As is clear from the previous discussions, this target would weigh 62.4 tons if it is located in the cavity at 500 m from the interaction point or 2.4 tons if it is located in the space between and around the beam pipes starting at 100 m from the interaction point.

A rather different approach would be that of a fixed-target experiment. The choice here is between a (costly) beam dump, a dedicated gas-jet target, and the exploitation of *parasitic* neutrino beams produced in the beam scrapers. The latter are hollow annular plugs inserted in the beam pipes to reduce the beam halo. Again, we will assume that a detector of 2 mrad transverse size, a length of 40 m, and an average density of 2 g/cm^3 can be located 100 m away from a scraper.

Needless to say, the results of our Monte Carlos can be understood without a Monte Carlo. We shall not dwell here in analytical approximations, but we offer some preliminary comment on the numbers we obtain, by way of example. In the beam-beam mode, the time-integrated number of D_s^+-prompt-decay ν_τs in one hemisphere is, in a self-explanatory notation:

$$N_{\nu_\tau} = \sigma(pp \to D_s^+)\, B.R.(D_s^+ \to \tau^+\nu_\tau)\, \frac{1}{2} \int L\, dt. \qquad (10)$$

The number of $\bar{\nu}_\tau$s in the subsequent τ^+ decay is the same. For the fixed-target mode, the corresponding number in the forward hemisphere (towards which, to a good approximation, all neutrinos go) is:

$$N_{\nu_\tau} = \frac{\sigma(pp \to D_s^+)}{\sigma_{tot}(pp)}\, B.R.(D_s^+ \to \tau^+\nu_\tau) \int N_p\, dt, \qquad (11)$$

where N_p is the rate at which protons are intercepted (in a beam-dump mode we would be neglecting the softer neutrinos made by secondaries).

Let

$$\sigma_{\nu(\bar{\nu})}(E_{\nu(\bar{\nu})}) = \sigma^0_{\nu(\bar{\nu})}\, 10^{-38}\, E_{\nu(\bar{\nu})}\ \mathrm{GeV}^{-1}\ \mathrm{cm}^{-2}, \qquad (12)$$

(with $\sigma^0_\nu = 0.63$ and $\sigma^0_{\bar{\nu}} = 0.32$) describe the CC neutrino cross-sections on an approximately isoscalar target. Let N_A be Avogadro's number, ρ the target density and L_d the

detector's length. Let χ be the fraction of neutrinos that reach our standard target and let X be the fraction of the target's length that these neutrinos traverse, both of them averaged over neutrino energy. To a good approximation the total number of CC ν_τ events from the $D_s^+ \to \tau^+\nu_\tau$ branch is:

$$n(D_s^+ \to \nu_\tau) \;=\; N_{\nu_\tau}\,\chi\,X\,\sigma_\nu^0\,\langle E_\nu\rangle\,N_A\,\rho\,L_d, \tag{13}$$

with a similar expression holding for the $\bar{\nu}_\tau$-induced events from the $D_s^+ \to \tau^+ \to \bar{\nu}_\tau$ branch.

As an example, assume a "year" (10^7 s) of running in beam-beam mode at the LHC, with an average luminosity of $L_{LHC} = 2\times10^{34}$ cm^{-2} s^{-1}. Take $\sigma(pp \to D_s^+) = 1$ mb, as in the $\alpha_\psi = 0$ variant of the QGSM. Read $\langle E\rangle$ from Table 3, χ and X from Table 4 and $B(D_s^+ \to \tau\nu_\tau)$ from Table 2, to obtain the estimate

$$\begin{aligned} n(D_s^+ \to \nu_\tau) &\sim 110 \\ n(D_s^+ \to \bar{\nu}_\tau) &\sim 550 \end{aligned} \tag{14}$$

The total $\nu_\tau + \bar{\nu}_\tau$ rate is approximately the double of the sum of the above numbers, as the neutrinos from the production and decay of D_s^- have to be added to them.

In Table 5 we give the results of a full Monte-Carlo calculation of the number of neutrino interactions per "year" for our generic detector in the four cases considered. For the currently expected LHC and SSC luminosities, we have taken the values $L_{LHC} = 2\times 10^{34}$ cm^{-2} s^{-1} and $L_{SSC} = 10^{33}$ cm^{-2} s^{-1}. For the fixed-target calculations we have assumed a total of 5×10^{17} protons on target per year of running for the LHC, and 1×10^{17} for the SSC (compared with the LHC, the SSC is supposed to store one forth as many protons per beam, and we are assuming its full-cycle period to be a little longer).

Our predictions are meant to be somewhat pessimistic, given the very soft longitudinal-momentum and very hard transverse-momentum distributions characterizing our modelling of the very high energy production of charmed and beautiful particles. Even so, we expect one or two thousand $\nu_\tau + \bar{\nu}_\tau$ interactions per year (in our rather low-density standard detector) for the totally non-intrusive LHC beam-beam mode of operation, at the design luminosity. This is more than enough to clearly establish a clean ν_τ signal, though insufficient to do "ν_τ physics" at the level of precision we are accustomed to for other neutrino flavours. The rates for SSC are (assuming an identical set-up) reduced by about a factor of two, mainly because of the much lower assumed luminosity. Figure 19 indicates that the placement of our standard detector at the SSC, in the region were the beams diverge after a crossing, is not an unconceivable task, though its average distance to the interaction point may be 200 m, rather than the assumed 120 m for the LHC. It is straightforward to scale our results to detectors placed at different distances and/or with different column densities, provided their angular coverage stays put at some 2 mrad. The use of other angular apertures, on the other hand, would require one to redo the calculations, although Fig. 13 can help in an estimate of the result.

Table 5 indicates that the "fixed-target" modes (i.e. beam scrapers, a thin filament target, etc.) are a very atractive possibility, assuming as we are that one can peel off 5×10^{17} protons per year at the LHC and one fifth as many at the SSC. Here our predictions have a smaller spread and are more reliable than for the beam-beam mode, since they

involve much less of an energy extrapolation. While in the beam-beam mode the LHC is (by a modest factor of two due to the assumed luminosities) "the winner"; the opposite, by a similar factor, is true in the fixed-target option, all according to Table 5. The assumed relative scarcity of protons on a fixed target at the SSC is a little more than compensated by the higher D-production cross-section, and by the bigger boost and consequent neutrino energy, all at a mean $p_\perp$ that has not varied much from one machine to the other.

6 Conclusions

We have calculated the neutrino fluxes produced in beam-beam and beam-fixed-target interactions at the LHC and SSC by the production and prompt decay of charmed particles. We have used the QGSM to calculate the charm-production cross-section at high energy and a fit to existing data, based on the Hagedorn model, to foretell the charmed particles' transverse-momentum distribution. We use these fluxes to calculate the number of ν interactions per year in generic detectors subtending 2 mrad in the forward direction of the interaction regions.

A small detector located directly downstream of the interaction point, at about 100 m distance, would be exposed to a neutrino flux inducing a few thousand tau neutrino interactions per year, at the design luminosity of the LHC, a current $L_{LHC} = 2\times10^{34}$ cm^{-2} s^{-1}. The number of ν_e and ν_μ interactions will be a factor of 10 higher. Given the small size of the detector and with present detecting technologies, it seems possible, at a low cost, to identify the tau neutrino. An ambitious neutrino program up to TeV energies, for ν_e and ν_μ seems also feasible and could be carried out at a more distant location, some 500 m away from the interaction point. The tau neutrino could also be discovered at this more distant location, provided detection techniques, such as the "electronic bubble chambers" we have quoted [1],[28], could keep the price of a massive detector within reasonable bounds.

Acknowledgements

We thank Anna Pascual for help with implementing the program to compute the charm cross-sections with the QGSM. We had many useful discussions with Manuel Traseira who greatly contributed to our understanding of the approach to the computation of the mean $p_\perp$, and with Pilar Hernandez. A.B. Kaidalov introduced us to the mysteries of the QGSM. We also thank W. Scandale for his patient explanations about the LHC layout and M. Cavalli-Sforza for discussions on detectors and bakgrounds.

$\sqrt{s}$ (GeV)		$D^+ + D^-$	$D^0 + \bar{D}^0$	$D_s^+ + D_s^-$	$D + \bar{D}$
27.4	Data	12 ± 1	18 ± 2		30 ± 1
	QGSM ($\alpha_\psi = 0.$)	5	10	2	17
	QGSM ($\alpha_\psi = -2.2$)	6	14	3.5	27.5
38.8	Data	26 ± 4	22 ± 8		49 ± 9
	QGSM ($\alpha_\psi = 0.$)	9	15	5	29
	QGSM ($\alpha_\psi = -2.2$)	12	23	8	43
630.0	Data				680 ± 560
	QGSM ($\alpha_\psi = 0.$)	110	125	90	325
	QGSM ($\alpha_\psi = -2.2$)	255	300	245	800

Table 1: Comparison between data at various energies and the prediction of the QGSM for the total cross-section of charmed particle production. The agreement is seen to be slightly better for the $\alpha_\psi = -2.2$ variant of the model.

Decay channel	Branching ratio
$D^\pm \to \nu_e(\nu_\mu) + X$	0.19
$D^0(\bar{D}^0) \to \nu_e(\nu_\mu) + X$	0.08
$D_s^\pm \to \tau\nu_\tau$	0.04
$B \to \nu_e(\nu_\mu) + X$	0.20
$B \to \nu_\tau + X$	0.10

Table 2: Branching ratios used in our calculations. See text for references.

	123.2 GeV	197.7 GeV	16.0 TeV	40.0 TeV
ν_τ^1	465	795	620	1135
ν_τ^2	90	165	125	230

Table 3: Mean energy (in GeV) of the tau neutrinos produced in the decay $D_s \to \tau\nu_\tau$, and in the subsequent tau decay, interacting in our standard detector for the pp c.m. energies of interest.

	123.2 GeV	197.7 GeV	16.0 TeV	40.0 TeV
ξ	0.025	0.075	0.01	0.028
X	0.7	0.8	0.7	0.8

Table 4: ξ and X (see text) for the decay $D_s \to \tau\nu_\tau$, and the subsequent tau decay, at the four energies considered.

$\nu + \bar{\nu}$ interactions	$QGSM$ variant	123.2 GeV	197.7 GeV	16.0 TeV	40.0 TeV
$\nu_l + \bar{\nu}_l$ (charm + beauty)	$QGSM_1$	17100	27400	11700	6700
	$QGSM_2$	21500	38300	15000	10700
$\nu_l + \bar{\nu}_l$ (charm only)	$QGSM_1$	16750	26800	11400	6500
	$QGSM_2$	21100	36600	14900	10600
$\nu_\tau + \bar{\nu}_\tau$ (charm + beauty)	$QGSM_1$	1400	2600	1150	650
	$QGSM_2$	1950	4440	1750	1300
$\nu_\tau + \bar{\nu}_\tau$ (charm only)	$QGSM_1$	1250	2240	1050	575
	$QGSM_2$	1800	3700	1700	1250

Table 5: Number of charged current neutrino plus antineutrino interactions per year in our standard detector for the energies considered and the two variants of the model ($QGSM_1$ stands for $\alpha_\psi = 0$ ($\alpha_\Upsilon = 0$), while $QGSM_2$ stands for $\alpha_\psi = -2.2$ ($\alpha_\Upsilon = -8.$). The symbol ν_l stands for ν_e or ν_μ. The ν_τ entries include both the ν_τ^1 and ν_τ^2 neutrino contributions.

References

[1] P. Astier et al., CERN-SPSLC/91-21. SPSC/P261 (1991).

[2] Charm II Collaboration, Proposal CERN-SPSC/90-42.

[3] K. Kodama et al., Draft Proposal. FNAL P803.

[4] A. De Rújula and R. Rückl, "Neutrino and Muon Physics in the Collider Mode of Future Accelerators", CERN-TH-3892/84.

[5] R.J.N. Phillips, Proc. Twentieth International Conference on High Energy Physics, Madison, (1980).

F. Halzen, Proc. Twenty-first International Conference on High Energy Physics, Paris, (1982).

[6] See, for instance, P. Nason, S. Dawson and K. Ellis, Nucl. Phys. B303 (1988) 607, B327 (1989) 49, and B335 (1990) 260.

[7] R. Hagedorn, CERN Report 71-12 and references therein.

[8] G. 't Hooft, Nucl. Phys. B72 (1974) 461.

[9] G. Veneziano, Phys. Lett. 52B (1974) 220.

[10] A.B. Kaidalov and K.A. Ter-Martirosyan, Sov. J. Nucl. Phys. 39 (1984) 979.

[11] Yu.M. Shabel'skii, Sov. J. Nucl. Phys. 44 (1986) 117.

[12] A.B. Kaidalov and O.I. Piskounova, Sov. J. Nucl. Phys. 45 (1985) 816.

[13] A.B. Kaidalov and O.I. Piskounova, Sov. J. Nucl. Phys. 43 (1986) 994.

[14] A.B. Kaidalov, Sov. J. Nucl. Phys. 45 (1987) 902.

[15] O.I. Piskounova, unpublished preprint, 1990.

[16] M. Aguilar-Benitez et al., Z. Phys. C31 (1986) 491.

[17] M. Aguilar-Benitez et al., Phys. Lett. B189 (1987) 476.

[18] M. Aguilar-Benitez et al., Phys. Lett. B201 (1988) 176., Z. Phys. C40 (1988) 321.

[19] R. Ammar et al., Phys. Lett. B182 (1986) 110.

[20] O. Botner et al., Phys. Lett. B236 (1990) 488.

[21] H. Koppe, Z. Naturforsch. 3A (1948) 251, Phys. Rev. 76 (1949) 688.

[22] E. Fermi, Progr. Theor. Phys. 5 (1950) 570.

[23] See V. Barnes in Proc. of the 24th Rencontres de Moriond, 1989, ed. Tran Thanh Van, and references therein.

[24] T. Sjöstrand and M. Bengtsson, Comput. Phys. Commun. 43 (1987) 367.

[25] J.J. Hernandez et al., Particle Data Group, Review of particle properties, Phys. Lett. B239 (1990) 1-516.

[26] M. Talebzadeh et al, Nucl. Phys. B291 (1987) 503.

[27] K. Winter, CERN-EP/89-182 (1989).

[28] L. Bassi et al., ICARUS I: An optimized, real time detector of solar neutrinos, LNF-89/005 (1989);
A. Bettini et al., The ICARUS Liquid Argon TPC: A complet imaging device for particle physics, LNGS-91/16 (1991).

[29] W. Scandale, CERN SL/91-03 (AP), LHC Note 139 (1991).

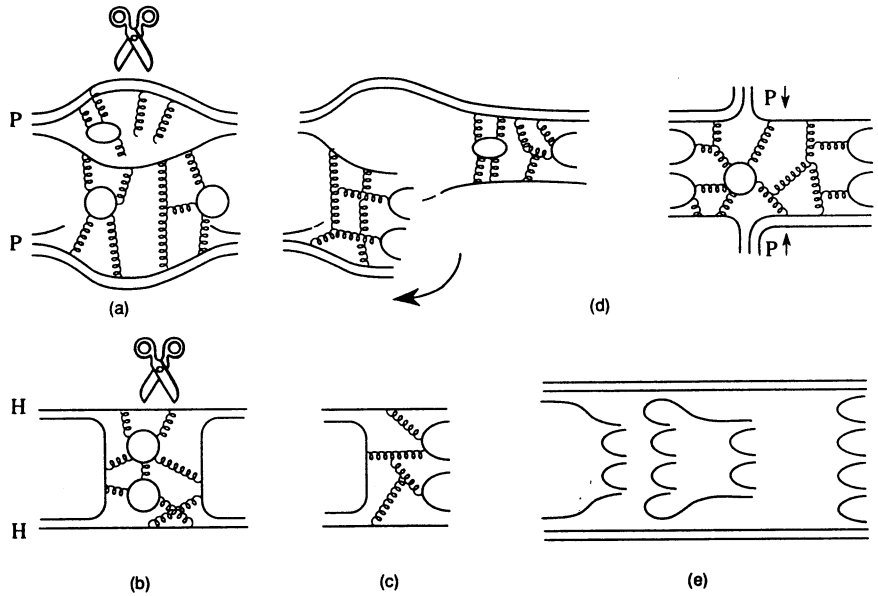

Figure 1: (a) Diagrams of cylindrical type. (b) Diagrams of planar type. (c) Cutting of planar diagrams. (d) Cutting of cylindrical diagrams. (e) Multi-pomeron processes.

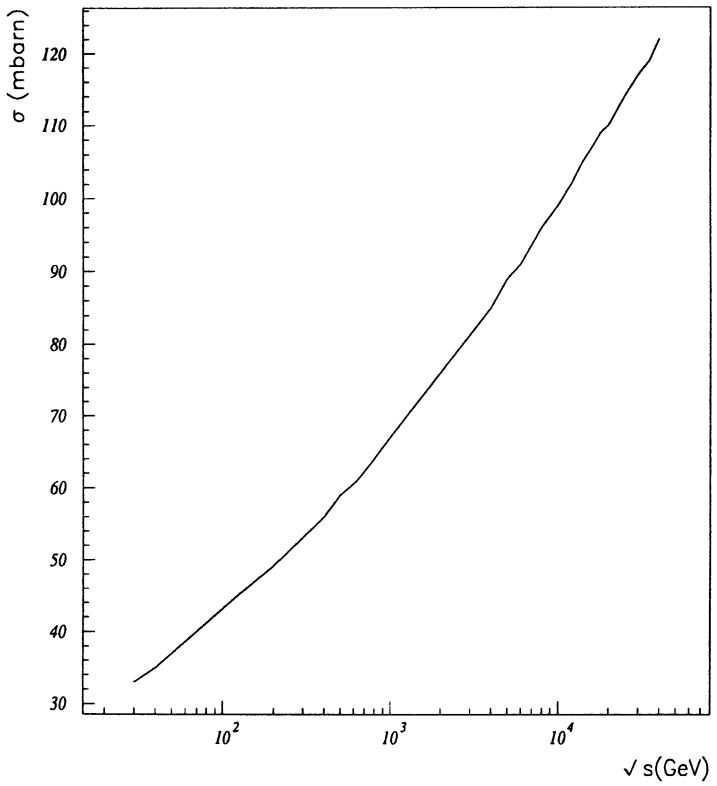

Figure 2: Variation of the total pp cross-section with energy in the QGSM.

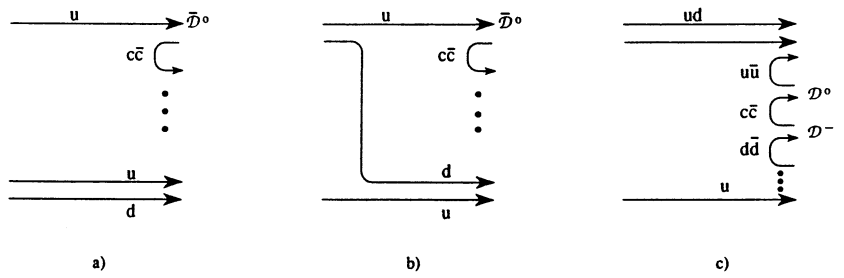

Figure 3: Fragmentation of quark chains into D mesons. (a-b) Favoured fragmentation into $\bar{D}^0$; (c) Unfavoured fragmentation into D^- and $D^0(D^+)$.

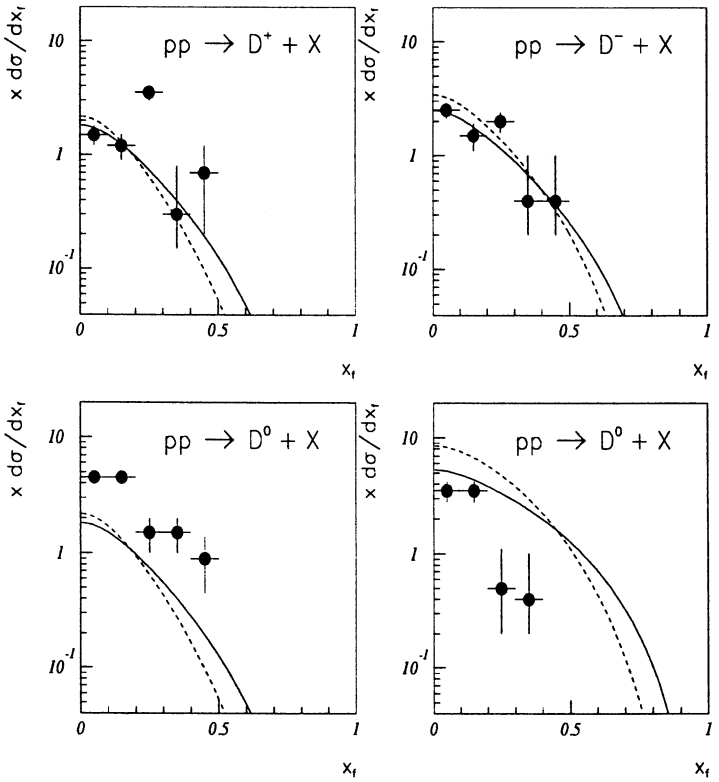

Figure 4: x distributions for the different D mesons measured at $\sqrt{s} = 27.4$ GeV together with the QGSM predictions for $\alpha_\psi = 0$ (solid line) and $\alpha_\psi = -2.2$ (dashed line).

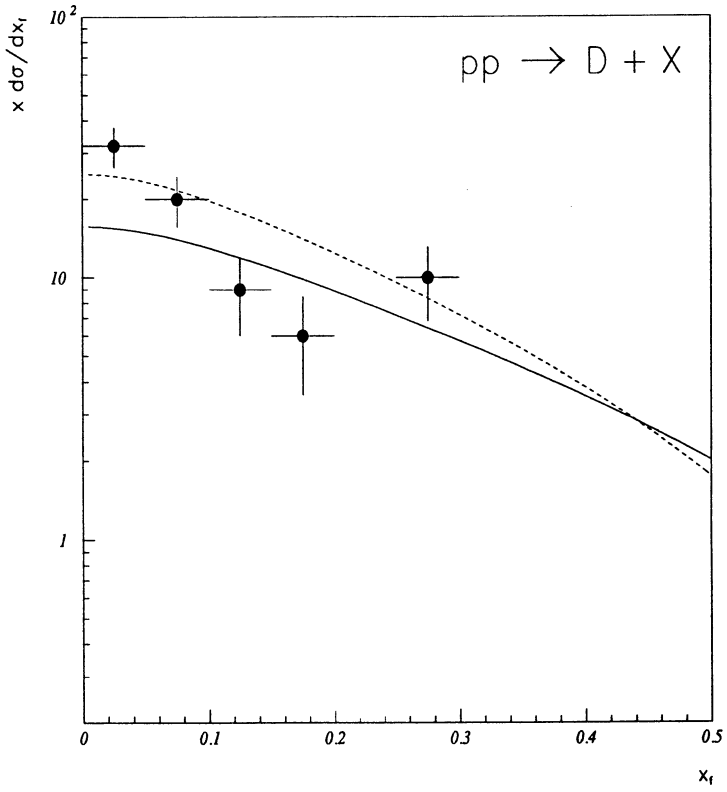

Figure 5: x distributions for the inclusive production of D mesons measured at $\sqrt{s} = 38.8$ GeV together with the QGSM predictions for $\alpha_\psi = 0$ (solid line) and $\alpha_\psi = -2.2$ (dashed line).

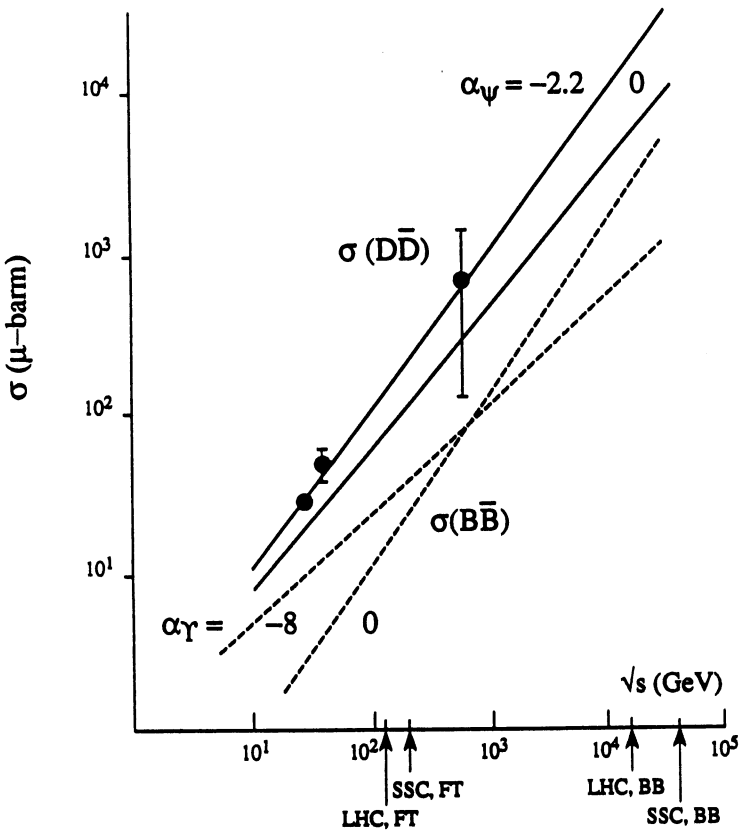

Figure 6: The continuous lines are QGSM predictions for the evolution of the total cross-section $\sigma(D\bar{D})$ with energy for $\alpha_\psi = 0$ and $\alpha_\psi = -2.2$. The points with error bars are the measurements at $\sqrt{s} = 27.4, 38.8$ and 630 GeV. The dashed lines are the predictions for the $\sigma(B\bar{B})$ total cross sections for $\alpha_v = 0$ and $\alpha_\psi = -8$.

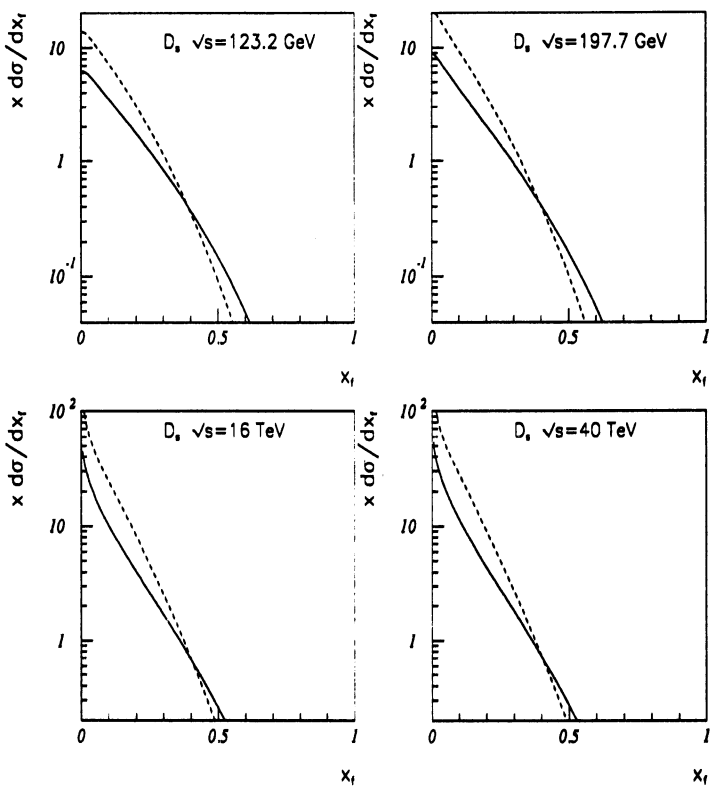

Figure 7: QGSM predictions for the x distributions of D_s mesons at (a) $\sqrt{s} = 123.2$ GeV, (b) $\sqrt{s} = 197.7$ GeV, (c) $\sqrt{s} = 16$ TeV, (d) $\sqrt{s} = 40$ TeV, for $\alpha_\psi = 0$ (solid line) and $\alpha_\psi = -2.2$ (dashed line).

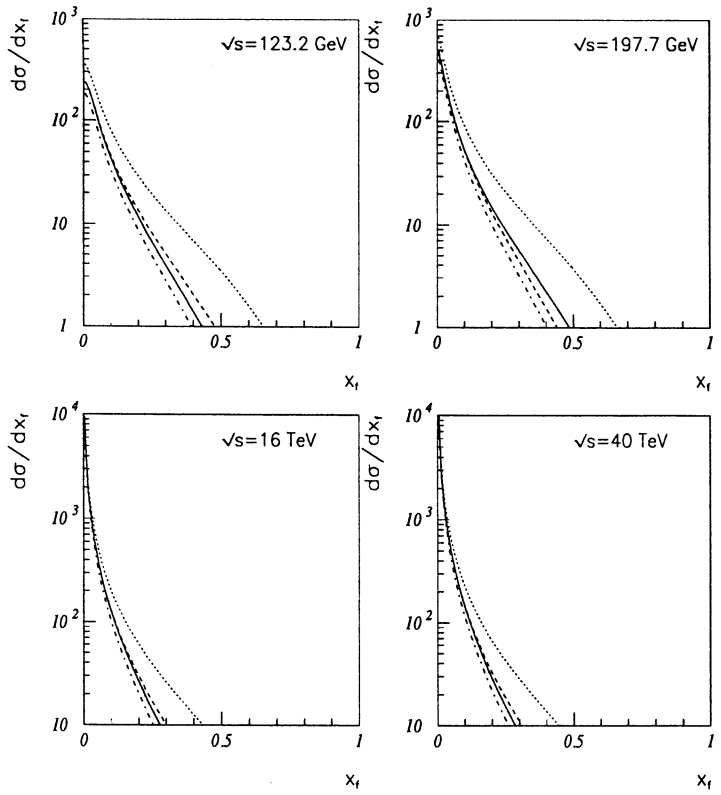

Figure 8: QGSM predictions ($\alpha_\psi = 0$) for the x distributions of D^+ (solid line), D^- (dashed line), $\bar{D}^0$ (dotted line) and D_s^+ (dash-dotted line) mesons at (a) $\sqrt{s} = 123.2$ GeV, (b) $\sqrt{s} = 197.7$ GeV, (c) $\sqrt{s} = 16$ TeV and (d) $\sqrt{s} = 40$ TeV.

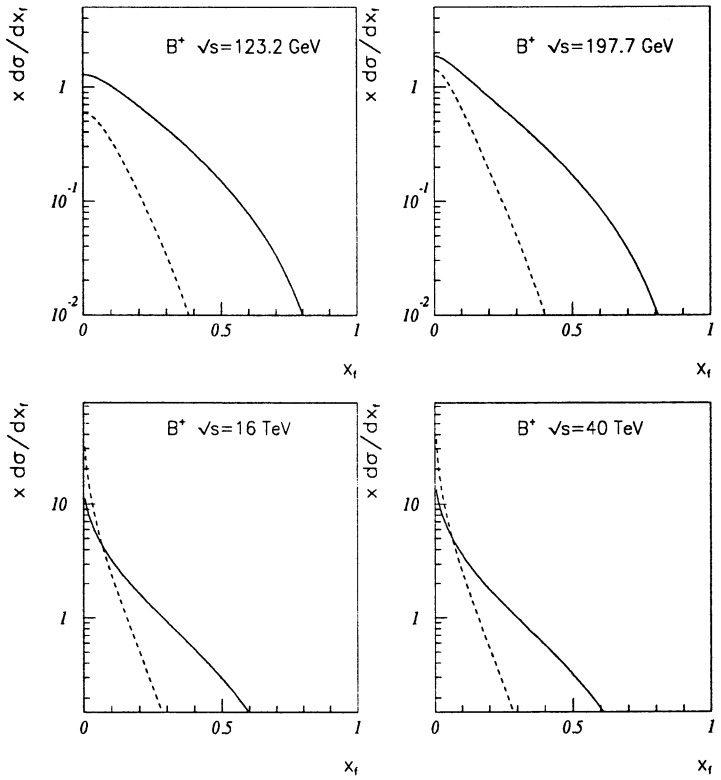

Figure 9: x distributions for beautiful mesons at (a) $\sqrt{s} = 123.2$ GeV, (b) $\sqrt{s} = 197.7$ GeV, (c) $\sqrt{s} = 16$ TeV, (d) $\sqrt{s} = 40$ TeV. Solid and dashed lines correspond to $\alpha_\Upsilon = 0$ and $\alpha_\Upsilon = -8$ respectively.

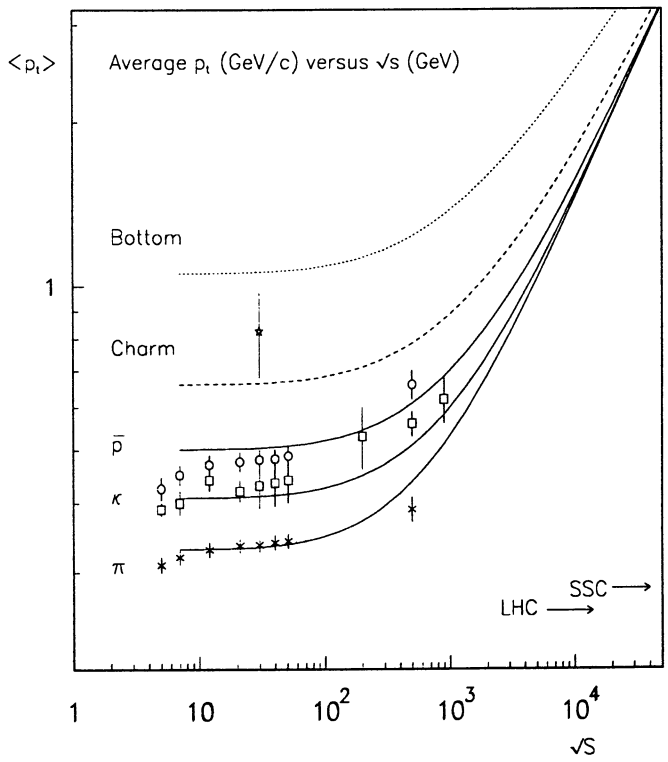

Figure 10: Fits with the empirical expression (9) to existing data and extrapolation to higher energies.

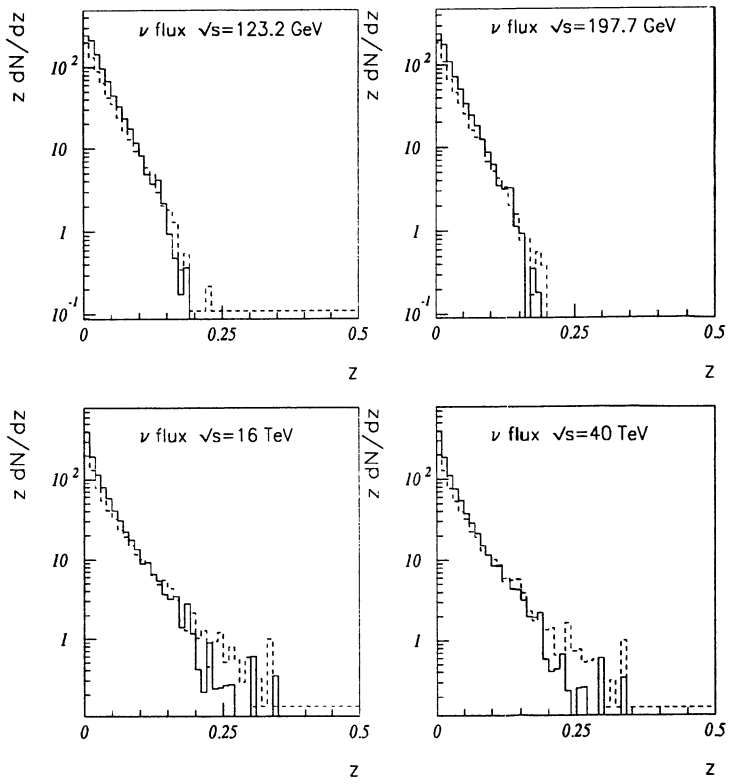

Figure 11: $z_\nu dN/dz_\nu$ distributions for: (a) $\sqrt{s} = 132$ GeV, (b) $\sqrt{s} = 198$ GeV, (c) $\sqrt{s} = 16$ TeV, (d) $\sqrt{s} = 40$ TeV.

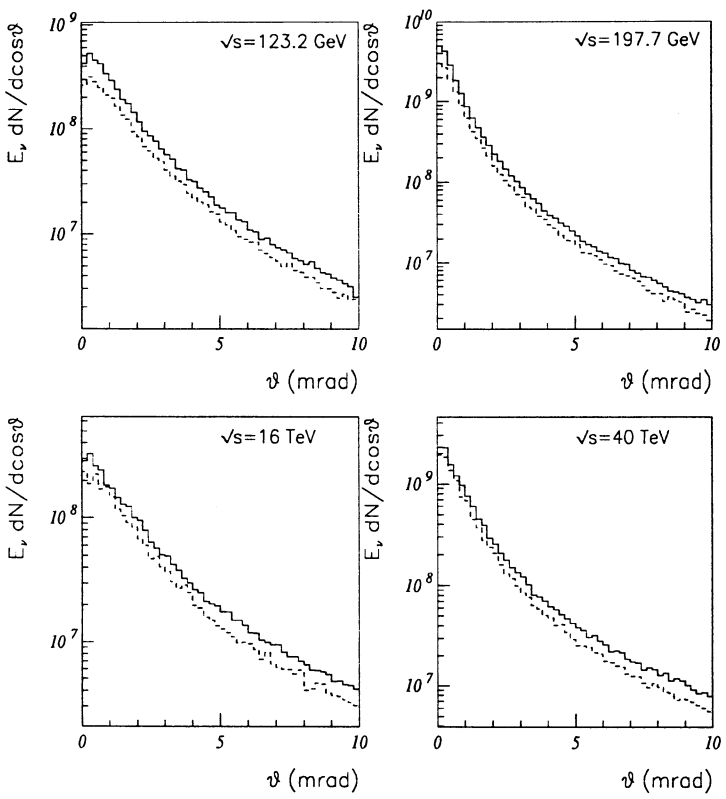

Figure 12: $E_\nu dN/d\cos\theta$ distributions for: (a) $\sqrt{s}$ = 132 GeV, (b) $\sqrt{s}$ = 198 GeV, (c) $\sqrt{s}$ = 16 TeV, (d) $\sqrt{s}$ = 40 TeV. Solid line is for the variant 1 of the QGSM. Dashed line is for the variant 2.

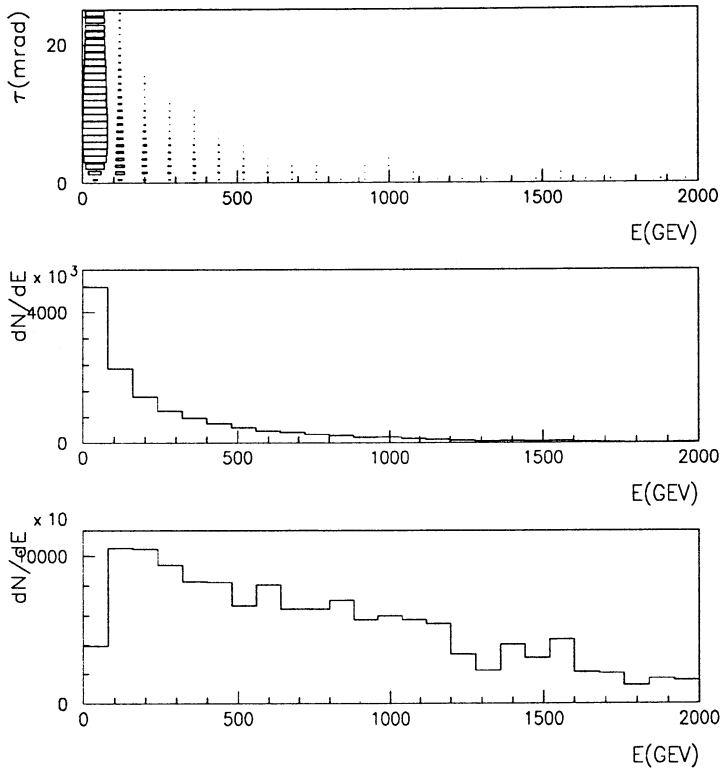

Figure 13: Some properties of a ν_τ beam produced in LHC collisions. The decay $D_s \to \tau\nu_\tau$ and the subsequent τ decay are taken as an example. (a) Neutrino emission angle versus neutrino energy; (b) emitted neutrino's energy; (c) energy of the neutrinos intercepted by a 2 mrad-wide target, where the "soft" and the "hard" neutrino components of the beam can be somewhat distinguished.

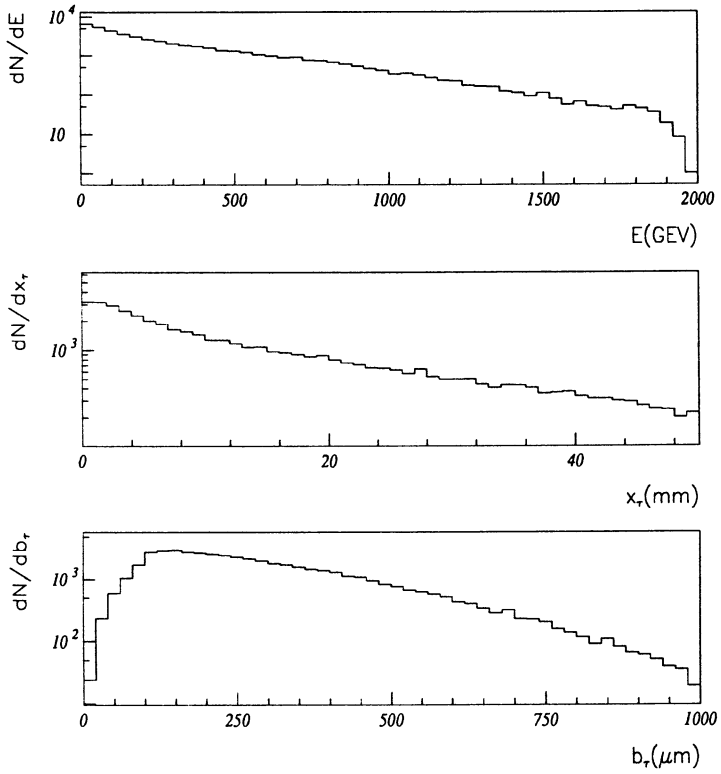

Figure 14: (a) Energy of the τ's produced by a CC ν_τ interaction in our standard detector. (b) Mean free path x_τ. (c) Mean transverse decay length.

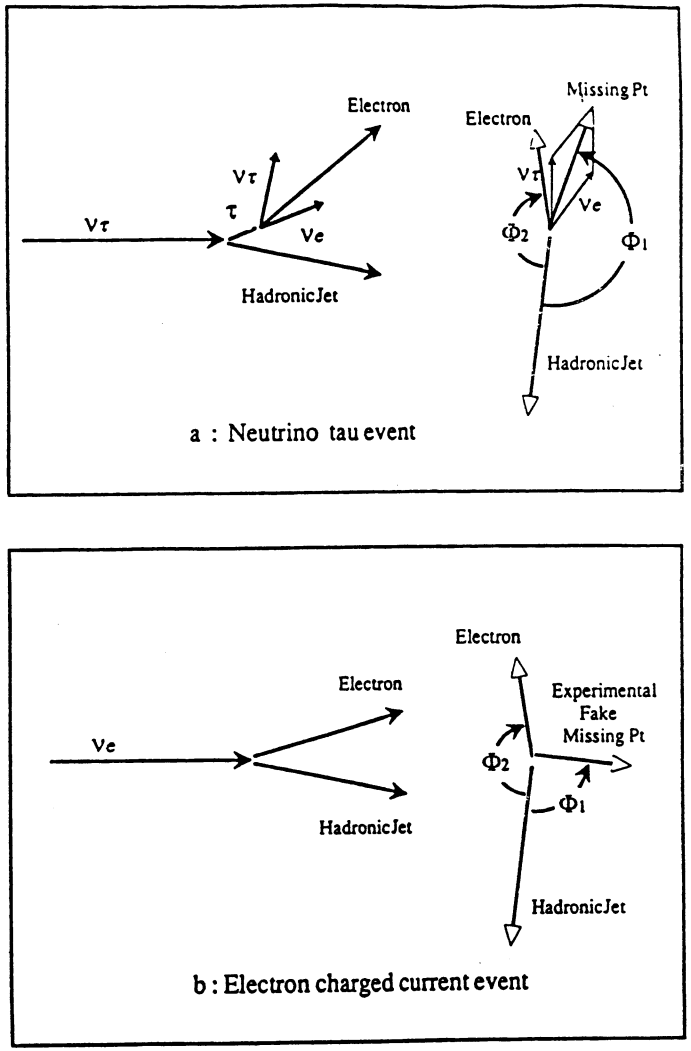

Figure 15: Definition of the $(\phi_{\mu,h}, \phi_{m,h})$ angles used to characterize a ν_τ interaction. This figure has been taken from ref. 1.

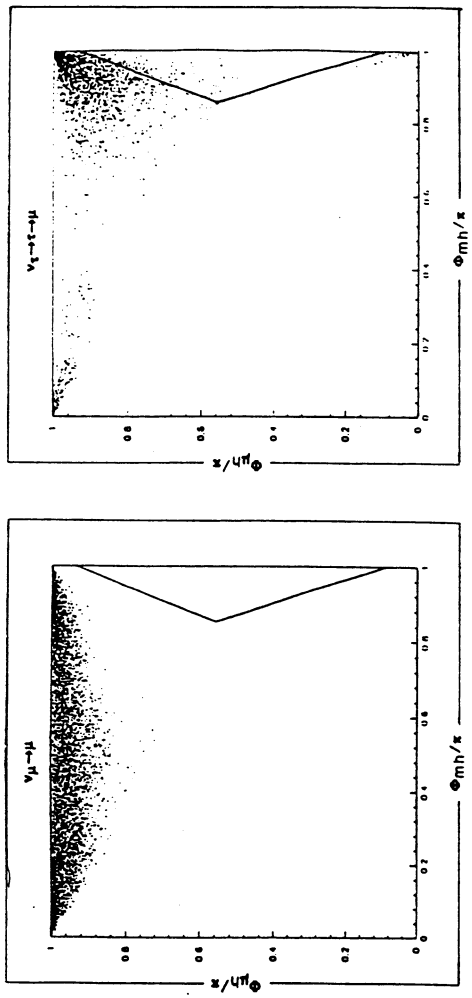

Figure 16: Scatter plots of the angle in the transverse plane between the $P_{\perp}^{miss}$ and the total momentum of the hadron jet, versus the corresponding angle between the lepton (e or μ) and the hadronic jet. The curve shows the region where ν_τ interactions can be detected with high efficiency and very low background. See ref. 1.

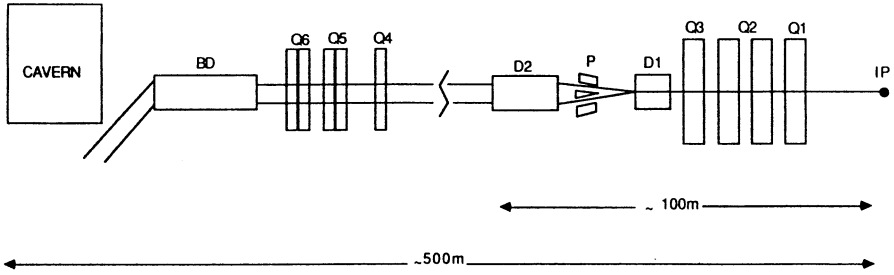

Figure 17: Design of one half of an LHC straight section. D's and Q's are dipoles and quadrupoles. IP is the intersection point. P is a "plug". BD is the first dipole bending the two beams at the start of an accelerator arch.

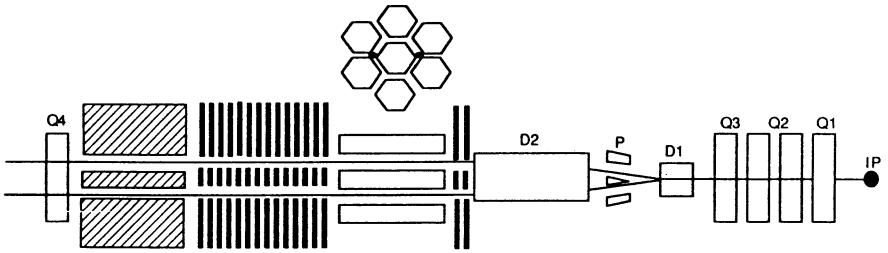

Figure 18: Artist's view of a possible detector layout very close to an interaction point in between and around the proton beam pipes. Notation is as in Fig. 17. The dotted elements (also seen in the transverse view) are the active target. The remaining elements stand for trackers and calorimeters.

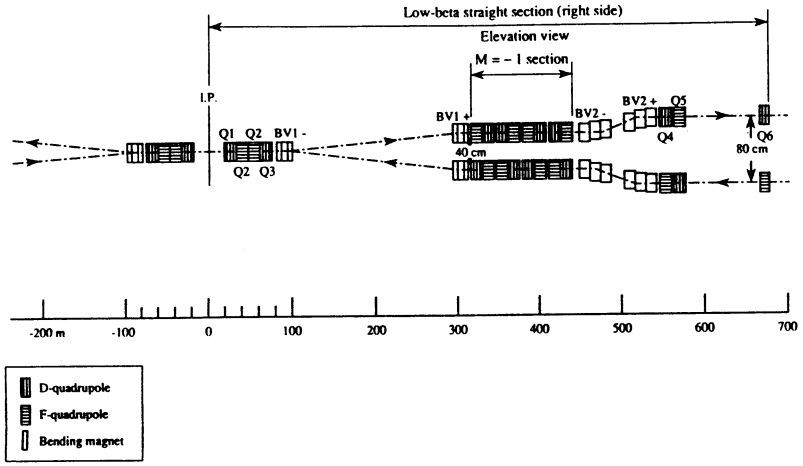

Figure 19: Design of an SSC interaction region.